8th International Symposium on Magnetic Bearing
August 26-28, 2002, Mito, Japan

ROBUST STABILITY OF THE LORENTZ-TYPE SELF BEARING SERVOMOTOR

Lyndon Scott Stephens, Hooi-Mei Chin
University of Kentucky, Bearings and Seals Laboratory
Department of Mechanical Engineering
521 CRMS, Lexington, KY 40506
stephens@engr.uky.edu

ABSTRACT

Robust stability and closed loop performance of a Lorentz-type self bearing servomotor test rig are presented. Previous work has identified the existence of multiple destabilizing terms in the servomotor force-torque characteristic. These terms are treated as modeling errors and accounted for using structured uncertainty. A set of decoupled PD controllers is designed and the stability robustness of the system is evaluated via μ-analysis. Experimental results confirm that the resulting controllers provide stable levitation and angular pointing of the rotor over all uncertainties. The closed loop bearing stiffness for the servomotor was measured as 502 N/mm and the closed loop angular position stiffness was measured as 17.7 N-m/A. The angular pointing accuracy of the servomotor was also measured and found to be <30 μrad.

INTRODUCTION

The Lorentz self bearing motor in this work is a servomotor that has been designed for use in precision pointing systems that require low weight and power. Space based systems such as laser cross-links and infrared sensors are examples of such applications [1]. In these applications the weight of the servomotor is minimized by combining the motoring and magnetic bearing function into a single actuator that uses common coils and flux return paths. A key design feature of the servomotor is that it is *slotless*. This increases pointing accuracy because it eliminates detent rotor positions (saliencies) and reduces cogging torque and torque ripple [2].

The Lorentz-type self bearing motor produces *both* motoring torque and bearing force using Lorentz-type forces. This approach to magnetic levitation was identified in [3] as a type 8 actuator. By contrast, other PM based self bearing motors are hybrid designs [4,5,6] that use Lorentz forces to generate motoring torque, and Maxwell (reluctance-type) forces to generate bearing force. Due to this construction, the hybrid designs suffer a tradeoff in bearing force and motoring torque with PM thickness as thicker permanent magnets lead to larger torque but increase the path reluctance for the bearing flux leading to smaller bearing forces. The main advantage of the Lorentz type design is that it eliminates this tradeoff and results in an actuator with simultaneously large motoring torque and bearing force. Work in Japan and Korea [7] has also progressed on Lorentz type designs that use slotted stators.

In previous work, the authors presented the theory of force and torque generation for the slotless Lorentz design [8,9,10]. That work quantified several destabilizing terms in the actuator force-current displacement relationship. These terms were found to consist of two types: i) cross-couplings between the x, y and θ direction bearing forces and torque; and ii) periodic variations in the current gains with rotor angular position. One approach the authors recommended is to treat these terms as uncertainties and synthesize controllers that are robustly stable.

Uncertainty models may take the form of structured or unstructured perturbations on a nominal system model, and these perturbations may be real (parametric uncertainty) or complex (uncertain system dynamics). Generally, unstructured uncertainty bounds the magnitude of all possible perturbations with no regard as to the location of the perturbations. This bounding, however, may be too conservative in the controller design because it relies solely upon the transfer function ∞–norm. For multiple uncertainty sources, the ∞–norm loses the structure of the uncertainty and allows for cross coupling between variables that may not exist. This results in conservative perturbations. On the other hand, structured uncertainty overcomes this conservatism by maintaining the

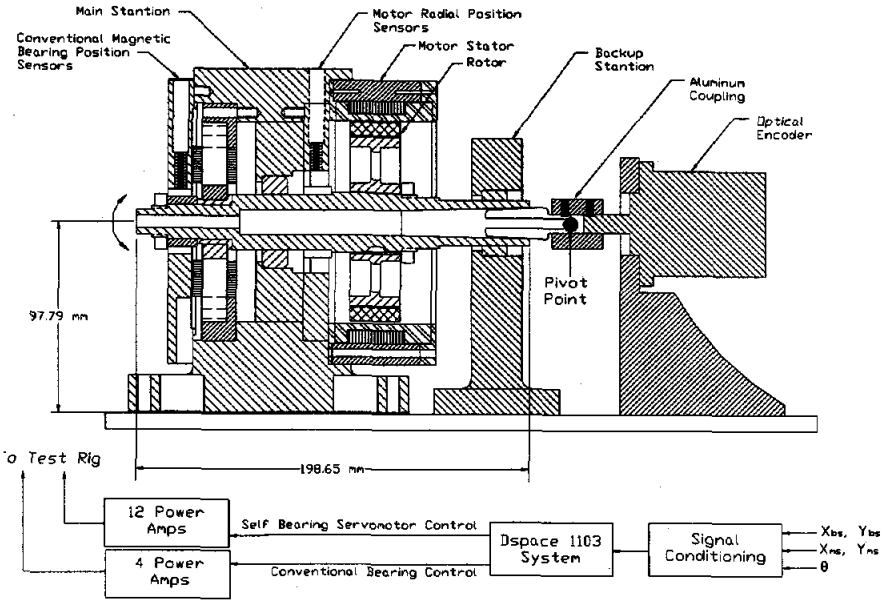

FIGURE 1: Lorentz self bearing servomotor test rig

location of the variations in the system model and preventing the cross coupling effect if one does not exist. The tool used for evaluating robust stability in the face of structured uncertainty is the structured singular value, μ, which represents the inverse of the smallest perturbation that results in instability [11]. For a system where M represents the nominal closed loop system and Δ represents the normalized plant uncertainty, robust stability is satisfied if $\mu(M)<1$. This relationship is defined mathematically in [11]. The mathematical basis is well documented and beyond the scope of this paper. Suffice it to say that robust stability is guaranteed for all uncertainties as long as the structured singular value, μ, is less than unity. A second useful definition is that the uncertainty when $\mu=1$, is the maximum uncertainty in the system before the onset of instability.

In previous work, the authors presented an experimentally verified nominal system model for the Lorentz servomotor test rig [12]. The present paper presents the structured uncertainty models for the system and uses the robust stability test in an iterative procedure to synthesize a set of PD controllers that maintain stability over all uncertainties. Experimental results are presented that demonstrate robust stability of the servomotor for all rotor angles, and quantify closed loop performance parameters.

TEST RIG DESCRIPTION

Figure 1 shows the Lorentz self bearing motor test rig and the feedback loop components. The rig consists of a conventional 8-pole active magnetic bearing (AMB) on the outboard end of a shaft (outboard is the end furthest from the encoder) with inductive probes measuring radial displacements, $x_{b,s}$ and $y_{b,s}$. The slotless self bearing motor is assembled near the mid span of the shaft and uses inductive probes to measure the radial displacements $x_{m,s}$ and $y_{m,s}$. The opposite end of the shaft is connected to a rotary optical encoder providing the angular position and velocity measurements, θ and ω. The coupling connection uses a Jarno interface and an aluminum coupling such that the encoder ball bearings support one end of the shaft through the coupling, while the other end of the shaft is free to move radially, pivoting about the coupling as illustrated in the figure.

The feedback loop of the system consists of five sensor measurements, $x_{b,s}$, $y_{b,s}$, $x_{m,s}$, $y_{m,s}$, and θ that are conditioned and fed into a D-space rapid control prototyping system that is used to implement the controllers for the conventional AMB and the self bearing motor. A group of 16 PWM transconductance power amplifiers generate the self bearing motor and the conventional AMB control currents.

Dynamic modeling of the system for controller design requires detailed models for the shaft rotordynamics, the self bearing servomotor, sensors, power amplifiers and the controller. Figure 2 shows the block diagram used to model the system including structured uncertainty. The nominal system model and uncertainty model for each component is discussed in the following sections. The matrices $[T_1]$-$[T_6]$ in Figure 2 are transformation matrices used to select the correct inputs and outputs for each transfer function block.

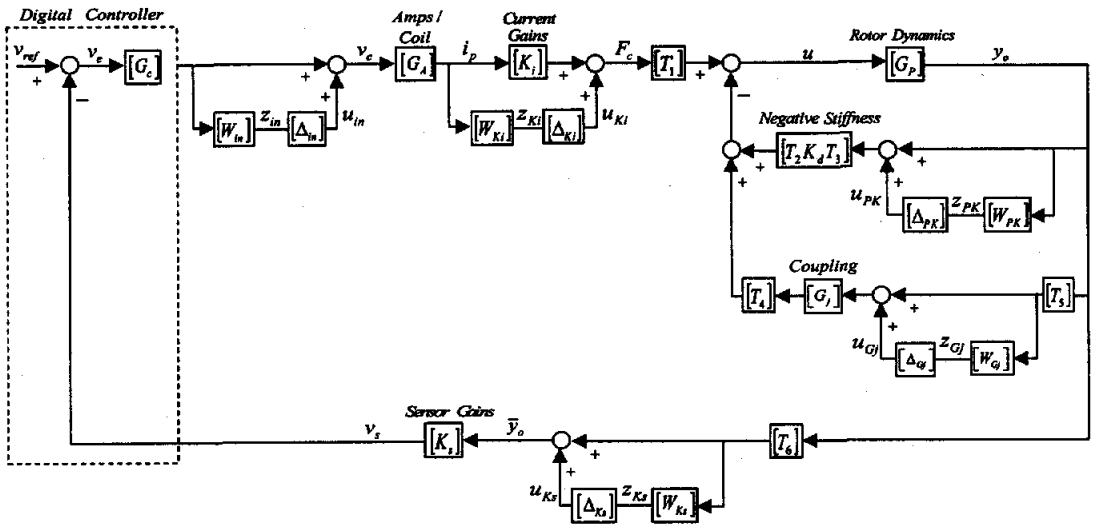

FIGURE 2: Linearized system block diagram with model uncertainty

SYSTEM MODEL

The nominal system model for this test rig was developed and experimentally verified in references [10,12]. The relevant components of this model are summarized in this section along with a detailed development of the uncertainty model. Table 1 summarizes the uncertainties and their weighting functions. As this table indicates, all weighting functions are independent of frequency, and both real and complex uncertainties are used resulting in a mixed μ robust stability test.

TABLE 1: Mixed μ Uncertainty Models

Uncertainty	Type	Weight
Δ_{in}	Complex	W_{in}=.03
Δ_{Ki}	Real	W_{Kixx}=0.10, W_{Kixy}=0.16, $W_{Ki\theta}$=0.10
Δ_{PK}	Complex	W_{plant}=0.15, W_{Kqxx}=0.03 W_{Kqxy}=0.03
Δ_{Gi}	Complex	W_{Gj}=0.05
Δ_{Ks}	Real	W_{Ks}=0.02

Rotordynamics

The lateral rotordynamic model of the shaft was generated using 35 lumped mass stations connected by massless springs and neglecting gyroscopics. For angular motion of the shaft, a single rigid body decoupled mode is also included. The dynamic equations are readily converted to 2*(2N+1) (N=35) first order ordinary differential equations and then reduced by truncating all lateral vibration modes except the rigid body modes (bouncing and tilting) and the first six flexible modes. The reduced order model is then of the form:

$$\ddot{\mathbf{z}} = [A]\mathbf{z} + [B]\mathbf{u} \tag{1}$$

$$\mathbf{y}_o = [C]\mathbf{z} \tag{2}$$

where $\boldsymbol{z}$ is the state vector, $\boldsymbol{u}$ is the vector of force inputs and $\boldsymbol{y_o}$ is the vector of displacement outputs. The rotordynamic transfer function matrix, $[G_p]$ of Figure 2, relating the displacement outputs, y_o, to the force inputs, $\boldsymbol{u}$ is computed using the resolvent. The outputs of interest are the displacements at the self bearing motor sensor locations, $x_{m,s}$ and $y_{m,s}$, the Jarno coupling connection point, x_j and y_j and the angular orientation of the shaft, θ. The inputs of interest are the corresponding force inputs due to the self bearing motor, $F_{x,m}$ and $F_{y,m}$, the Jarno coupling connection, $F_{x,j}$ and $F_{y,j}$ and the self bearing motor torque, T_θ. The input and output vectors for the rotordynamic model in Figure 2 are then:

$$\mathbf{y}_o = \begin{bmatrix} x_{m,s} & y_{m,s} & x_j & y_j & \theta \end{bmatrix}^T \tag{3}$$

$$\mathbf{u} = \begin{bmatrix} F_{x,m} & F_{y,m} & F_{x,j} & F_{y,j} & T_\theta \end{bmatrix}^T \tag{4}$$

The test rig shaft is connected to the encoder shaft through the Jarno coupling. Referring to Figure 1, it is assumed that the coupling provides a lateral stiffness and some structural damping for the shaft, but allows the shaft to pivot angularly about a point. The coupling is modeled in Figure 2 using the transfer function matrix, $[G_j]$, that simply provides the lateral stiffness and damping.

The main errors in the rotordynamics model are due to the simplified jarno coupling model and the fact that the encoder shaft and bearings are completely

neglected. To account for these errors, Figure 2 shows a complex additive uncertainty, Δ_{PK}, that includes a weighting function, W_{plant}=15% (see Table 1), on the diagonal terms to account for unmodeled dynamics. (Δ_{PK} also includes the uncertainty in the actuator negative stiffness matrix. This is why it is additive.) A second complex multiplicative uncertainty, Δ_{Gj}, is included with a weighting function of W_{Gj}=5% to further account for errors in the Jarno coupling model.

Self Bearing Servomotor

Figure 3 shows the layout of the Lorentz self bearing motor consisting of M=8 permanent magnet pole pairs attached to the rotor and N_{seg}=4 individually controlled winding segments attached to the stator. Each winding segment in the motor is an arc of $\pi/2$ radians and is attached to a slotless back iron. The windings occupy N_s=12 stations along each winding segment ID with N_w=85 individual wires per station. As this figure indicates, each segment has a unique control current, i_1-i_4, that is commutated into three phases 120° apart to produce Lorentz type forces F_{1x}, F_{2y}, F_{3x} and F_{4y} (a total of 12 phases). Commutation of the motor windings is accomplished digitally using the D-space controller and is described further in [10]. Ref [10] also shows that if the 4 segment currents are related to the 3 directional control currents, $i_{x,m}$, $i_{y,m}$ and i_θ as shown in Figure 3, then independent bearing forces and motoring torque are generated for small rotor eccentricities. The resulting bearing force and motoring torque relationships are of the form:

$$\begin{bmatrix} F_{x,m} \\ F_{y,m} \\ T_\theta \end{bmatrix} = \underbrace{\begin{bmatrix} K_{ixx} \pm W_{Kixx} & \pm W_{Kixy} & \pm W_{Kix\theta} \\ \pm W_{Kixy} & K_{ixx} \pm W_{Kixx} & \pm W_{Kiy\theta} \\ 0 & 0 & K_{i\theta} \pm W_{Ki\theta} \end{bmatrix}}_{[K_{i,m}]} \begin{bmatrix} i_{x,m} \\ i_{y,m} \\ i_\theta \end{bmatrix}$$

$$+ \underbrace{\begin{bmatrix} K_{xx,m} \pm W_{Kqxx} & \pm W_{Kqxy} & 0 \\ \pm W_{Kqxy} & K_{xx,m} \pm W_{Kqxx} & 0 \\ 0 & 0 & 0 \end{bmatrix}}_{[K_{d,m}]} \begin{bmatrix} x_m \\ y_m \\ \theta \end{bmatrix} \quad (5)$$

where $[K_{i,m}]$ is the current gain matrix, $[K_{d,m}]$ is the negative stiffness matrix, K_{ixx} is the bearing current gain, $K_{i\theta}$ is the torque current gain, $K_{xx,M}$ is the negative stiffness due to the permanent magnets and W is the model uncertainty. The current gains for the self bearing motor can be computed as [10]:

$$K_{ixx} = \frac{2}{\sqrt{2}\pi R} K_{i\theta} = \frac{4\cos(M\gamma) M N_w B_m L}{3} \quad (6)$$

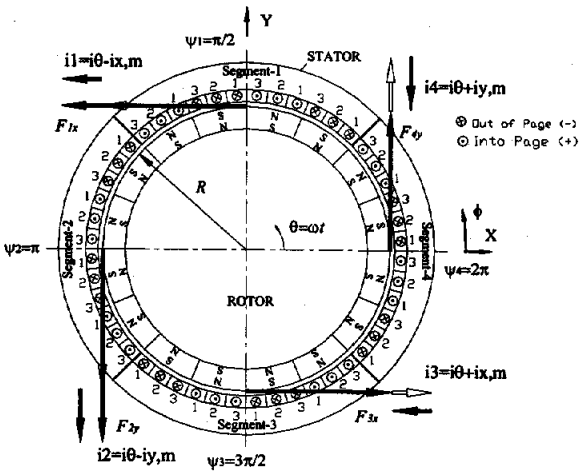

FIGURE 3: Self bearing servomotor layout

TABLE 2: Self bearing servomotor properties

Property	Symbol	Units	Value
Number of Pole Pairs	M	--	8
Number of Segments	N_{seg}	--	4
Phases per segment	N_ϕ	--	12
Radial Thickness of Permanent Magnets	t_m	*(mm)*	7.75
Radial Thickness of coil windings	t_c	*(mm)*	3.87
Nominal radial air gap	$g_{o,m}$	*(mm)*	0.762
Rotor Outer Radius	R	*(mm)*	50.8
Motor Length	L	*(mm)*	25.4
Peak Instantaneous Current per Phase	I_{pk}	*(Amps)*	12.0[1]
Max. Continuous Current per Phase	I_{rms}	*(Amps)*	3.0
Torque Gain	$K_{i\theta}$	*N-m/A*	3.5[2]
Bearing Force Direct Current Gain	K_{ixx}	*N/A*	28.9[2]
Bearing Capacity Peak/Continuous	F_{pk}/F_{cont}	*N*	350[1] / 85
Torque Capacity Peak/Continuous	T_{pk}/T_{cont}	*N-m*	42[1] / 11

[1]Limited by power amps, [2]Measured data

where R is the rotor radius, M is the number of PM pole pairs, N_w is the number of windings per station, B_m is the flux density due to the permanent magnets, L is the motor length and γ is the phase lag between the rotor angle and the coil current waveform. Table 2 summarizes the parameters for the self bearing servomotor including measured values indicating that K_{ixx}=28.9 N/A and $K_{i\theta}$ =3.5 N-m/A. The peak bearing load capacity of the servomotor in its present configuration is 350 N and is limited by the peak current of the power amplifiers. The motor can withstand peak currents up to 30 A. Under this condition, the peak bearing load capacity is 850 N.

The uncertainties in the force-current-displacement relation of equation (5) capture two destabilizing effects: (i) cross-coupling in both the current gain matrix and the negative stiffness matrix; and (ii) periodic variations in many of these terms with rotor angular position. These effects have been quantified in references in [10,12]. Table 1 summarizes the non-frequency dependent weighting functions for the uncertainty, Δ_{Ki}, and indicates that all uncertainties are treated as real parameter variations. Referring to Figure 2, an additive uncertainty representation is used for $[K_{i,m}]$. This is because several of the cross-coupled terms have a nominal value of zero. The uncertainty on K_{ixx} is W_{Kixx}= 10% which accounts for the periodic variation of this parameter with rotor angle and any variation due to modeling errors such as flux leakage. The uncertainty on $K_{i\theta}$ is $W_{Ki\theta}$=10% for the same reasons. The cross-coupled force gains have a nominal value of zero, but vary with rotor angle with a magnitude of 6% of K_{ixx}. W_{Kixy}=0.16 K_{ixx} was used to account for this and also includes 10% for flux leakage and other modeling errors. The cross-coupling between the x-θ and y-θ directions is negligibly small for this actuator under light-to-medium load conditions, therefore $W_{Kx\theta}$ and $W_{Ky\theta}$ are assumed to be zero.

The uncertainty in the actuator negative stiffness matrix is included in Δ_{PK} and is additive because the cross-coupled terms have nominal values of zero. The negative stiffness due the permanent magnets, $K_{xx,M}$, does not vary with angular position, but has some uncertainty due to the unknown amount of flux leakage and fringing. The flux due to the motor winding also creates a negative stiffness, but this term is very small when thick PM's are used (as in this actuator), therefore it is treated in the uncertainty. To account for these errors, an uncertainty of W_{Kqxx} =3% was used. The cross coupled negative stiffness terms are due to a Lorentz force imbalance that occurs when the rotor is in an eccentric position and a large torque is requested simultaneously. An uncertainty of W_{Kqxy}=0.03$K_{xx,M}$ is used to capture this effect.

Power Amps, Sensors and Controller

The power amplifiers are PWM transconductance amplifiers that drive the 12 phase coils of the servomotor. The frequency response of these devices were measured and fitted with a second order transfer functions, $[G_A]$, that account for the bandwidth and gain of the amps and the coil inductive load. The controllers are implemented on the D-Space motion control card. The rate of throughput for the card is much greater than the largest frequency of control. Therefore a continuous system model is used for the controller. Decoupled PD controllers are used on the servomotor to stabilize the shaft radial and torsional (angular) motion. The general form of the controller transfer function matrix is:

$$\underbrace{\begin{bmatrix} V_{cx,m} \\ V_{cy,m} \\ V_{c,\theta} \end{bmatrix}}_{v_c} = \underbrace{\begin{bmatrix} G_{PD,m} & 0 & 0 \\ 0 & G_{PD,m} & 0 \\ 0 & 0 & G_{PD,\theta} \end{bmatrix}}_{[G_c]} \underbrace{\begin{bmatrix} V_{ex,m} \\ V_{ey,m} \\ V_{e\theta} \end{bmatrix}}_{v_e} \quad (7)$$

where $G_{PD,m}$ and $G_{PD,\theta}$ are the PD controllers of the form $K_d s + K_p$.

The uncertainty in the power amplifiers, coil inductance and digital controller are lumped into a single, complex, input multiplicative uncertainty, Δ_{in}. The measured transfer functions for the amps and coil inductive load showed only 1% variation over all frequencies. Measurements for the digital controller showed an even smaller error. The weighting function used to account for these errors is W_{in}=3% which includes some extra uncertainty to guarantee a multivariable gain and phase margin at the input.

The x and y direction radial position sensors are inductive type probes and the θ direction motor angle sensor is an optical encoder. The bandwidths of these sensors are significantly larger than the bandwidth of any other sub-system, therefore they are modeled as pure gains on the diagonal of the 3x3 matrix, $[K_s]$. The nominal sensitivity of the self bearing motor inductive probes, and the encoder is 10 V/mm and 0.16 V/rad, respectively. The uncertainty in the radial sensors was measured as 2% over the range of the back-up bearing and that of the encoder was essentially negligible. This uncertainty is treated as a real parameter variation at the plant output, Δ_{Ks}, with a non-frequency dependent weighting function of W_{Ks}=2%.

ROBUST STABILITY

The objective of this work is to find a set of PD controller gains that stabilizes the rotor over all possible variations in system parameters. As previously discussed, this is accomplished by computing the structured singular value, μ, of the closed loop system, M, with respect to the system uncertainties. If μ(M)<1 over all frequencies then robust stability is said to be satisfied. The controller synthesis problem is then an iterative one, where a set of PD controller gains is found that stabilize the nominal system, then the closed loop system is tested for robust stability. If this test fails, then a new set of PD gains is found and tested. This process is repeated until a set of gains is found (none are guaranteed) that stabilize the rotor for all uncertain plants.

Figure 4 shows the robust stability μ plot for the servomotor test rig with the uncertainties in Table 1. The PD gains for the radial bearing control are K_p=6.0 and K_D=0.005, and for the angular (torque) control area K_p=35 and K_D=0.5. Since the maximum μ value is less than 1 over all frequencies, the mixed μ test indicates

that the system is robustly stable using these PD controller gains. This by no means represents the best gains but is just one set that maintains robust stability.

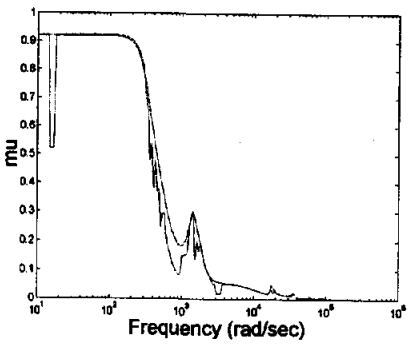

FIGURE 4: Robust stability test

RESULTS

The set of PD controllers was implemented on the experimental test rig such that the shaft was both levitated and held in a desired angular position using the self bearing motor. This was done without the aid of the conventional bearing. Figure 5 shows the closed loop transfer function (CLTF) for the servomotor x-direction bearing force ($G_{33,m}=V_{sx}/V_{ref,x}$). Both the measured and the theoretical (model based) transfer functions are shown. Good agreement is seen between the model and the experiment. This plot clearly shows that the flexible body modes of the system are below the noise floor in the experimental data. The bouncing mode for the shaft, and the system bandwidth (-45° point), occur at about 750 rad/s (120 Hz). A close examination of the figure indicates that the DC gain is 0.88 dB. One might expect the DC gain to be 0 DB (unity) in the x-direction (horizontal). This is not so because of the negative stiffness of the self bearing motor (Kxx,m=-101 N/mm). A handheld force gage was used to measure the closed loop bearing stiffness of the motor as 502 N/mm. Figure 6 shows the step response in the x-direction (horizontal) while the servomotor simultaneously holds the shaft angular position at θ=0° (the home position). The stable positive stiffness that the servomotor provides in the x-direction is evident.

Figures 7, 8 and 9 show the measured performance of the servomotor in the θ-direction (angular pointing) while simultaneously supporting the shaft as a magnetic bearing. Figure 7 shows the closed loop transfer function ($G_{55,cl}=V_{s\theta}/V_{ref,\theta}$). Both the experimental and theoretical plots are shown, indicating good agreement with the system model. The bandwidth (-45° point) in the θ-direction is about 90 rad/s (14.3 Hz) and the closed loop torsional stiffness results in a torsional vibration mode of about 80 rad/s (12.7 Hz). The reason for such a low bandwidth is the low bandwidth of the θ-

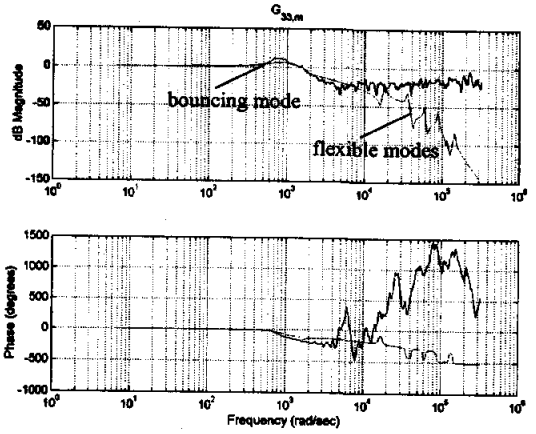

FIGURE 5: Servomotor CLTF in x-direction

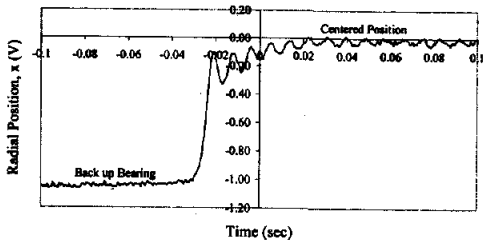

FIGURE 6: Servomotor step response in x-direction

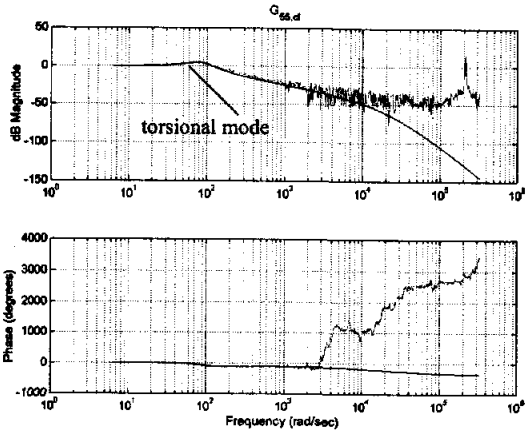

FIGURE 7: Servomotor CLTF in θ-direction

direction PD controller. Future work will focus on increasing this bandwidth without destabilizing the system. Figure 8 shows the step response of the servomotor when moving through an angle of π/2 rad (90°). Under this PD control, the rise time is 0.07 seconds, the angular slewrate is 38.5 rad/s (2205 deg/s) and the response is clearly overdamped. Finally, Figure 9 shows the harmonic response of the servomotor to a sinusoidal input of 1 Hz frequency and π/10 rad (18°) peak-to-peak amplitude. A handheld torque meter was used to measure the closed loop torsional stiffness of servomotor as 17.7 N-m/A.

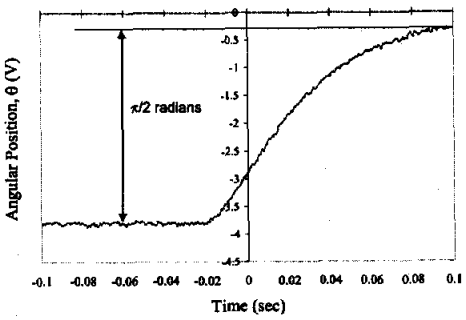

FIGURE 8: Servomotor step response in θ-direction

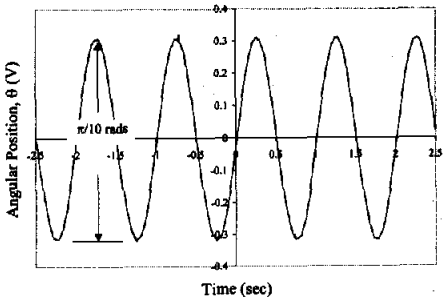

FIGURE 9: Angular Slewing at 1 Hz and π/10 rads

As a final experiment, the pointing accuracy of the servomotor was measured by steering a laser beam using a mirror attached to the shaft. The laser beam was incident on a fine grid located a large enough distance away such that fine motion of the beam could be measured. The pointing accuracy of the servomotor was found to be 30 μrad or better.

CONCLUSIONS

The experimental results clearly demonstrate the ability of the Lorentz-type self bearing servomotor to perform low frequency, smooth angular slewing and precision pointing while simultaneously levitating the rotor, in spite of the cross-coupled and angular position dependent nature of the force-current-displacement relationship. These results prove the utility of a structured uncertainty approach to synthesizing robustly stable controllers for the Lorentz self bearing servomotor. Future work will focus on further characterizing and improving the closed loop performance of the servomotor.

ACKNOWLEDGEMENTS

The authors express their appreciation to Airex Corporation of Dover, N.H., U.S.A., and to the United States Air Force for partial sponsorship of this research under contract F04701-98-C-0019.

REFERENCES

1. Carroll, D., Sedgewick, J., and Stephens, L.S., "Long Life, Fault Tolerant, Spacecraft Sensor Gimbal/Bearing System Final Report," United States Air Force Research Laboratory/VSDV, Contract No. F29601-98-C-0188, Mar, 1999.
2. Casemore, M.A. and Stephens, L.S., "Actuator Gains for a Toothless Permanent-Magnet Self-Bearing Motor," *IEEE Trans. on Magnetics,* vol. 35, No. 6, November, 1999.
3. Bleuler, H., "A Survey of Magnetic Levitation and Magnetic Bearing Types," *JSME International Journal*, Series III, Vol. 35, No. 3, 1992
4. Chiba, A., Rahman, M.A., and Fukao, T., "Radial forces in bearingless reluctance motor," *IEEE Trans. Magnetics,* vol. 27, p. 786, Mar. 1991.
5. Okada, Y., Miyamoto, S., and Ohishi, T., "Levitation and torque control of internal permanent magnet type bearingless motor", *IEEE Trans. Control Syst. Techn.,* vol. 4, no. 5, pp. 565-571, 1996.
6. Schoeb, R. and Bischel, J., "Vector control of bearingless motor", *Proc. 4th Int. Symp. Magn. Bearings,* ETH Zurich, Switzerland, pp. 327-332, 1994.
7. Okada, Y., Konishi, H., Kanebako, H., and Lee, C.W., "Lorentz Force Type Self Bearing Motor," *Proc. 7th Int. Symp. Magn. Bearings,* Zurich, pp. 353-358, August 2000
8. Steele, B.A. and Stephens, L.S., "A Test Rig for Measuring Force and Torque Production in A Lorentz, Slotless Self Bearing Motor", *Proc. 7th Int. Symp. Magn. Bearings,* ETH, Zurich, Switzerland, pp. 407-412, August, 2000
9. Stephens, L.S. and Kim, D.G., "Analysis and Simulation of a Lorentz-type, Slotless Self-Bearing Motor", *Proceedings of the 1st IFAC Conference on Mechatronics*, Darmstadt, Germany, September, 2000.
10. Stephens, L.S., and Kim, D.G., "Force and Torque Characteristics for a Slotless, Lorentz Self-Bearing Servomotor," To appear in IEEE Transactions on Magnetics, October, 2002
11. Doyle, J.C., "Structured Uncertainty in Control System," *Proc. IEEE Conf. Dec. Contr., Ft. Lauderdale,* 1985.
12. Stephens, L.S., "Dynamic Modeling and Validation of a Lorentz Self Bearing Motor Test Rig," *Proceedings of the ASME IGTI 2001 Conference*, ASME Paper No. 2001-GT-0567, June, 2001